Journal of Materials Chemistry A

High-temperature mixed potential CO gas sensor for in-situ combustion control

Journal:	*Journal of Materials Chemistry A*
Manuscript ID	TA-ART-06-2020-006320.R1
Article Type:	Paper
Date Submitted by the Author:	30-Aug-2020
Complete List of Authors:	Wang, Yi; West Virginia University, Department of Mechanical & Aerospace Engineering Ma, Liang; West Virginia University, Department of mechanical & aerospace engineering; Hebei University of Engineering, School of Materials Science and Engineering Li, Wenyuan; West Virginia University, Li, Wei; West Virginia University College of Engineering and Mineral Resources, Department of Mechanical and Aerospace Engineering Liu, Xingbo; West Virginia University, Department of Mechanical and Aerospace Engineering

ARTICLE

High-temperature mixed potential CO gas sensor for in-situ combustion control

Received 00th January 20xx,
Accepted 00th January 20xx

DOI: 10.1039/x0xx00000x

Yi Wang,‡[a] Liang Ma,‡[a,b] Wenyuan Li,[a] Wei Li[a] and Xingbo Liu*[a]

An in-situ, accurate and robust sensor that can sustain high temperature of above 1000°C is needed for on-site combustion monitoring because it can give real-time and local data to the control system to adjust the overal combustion efficiency. In this work, we find that nickel oxide (NiO) is a promising sensing material to CO which is a direct indicator of the status of combustion process of a power plant. Under the conditions of 0.5%-3% O_2 and 1000°C, the fabricated yttrium-stabilized zirconia (YSZ)-based mixed potential sensor using porous NiO demonstrates good sensitivity to CO, showing a signal as high as 36 mV to 1000 ppm CO. The effects of gas transport, structure and geometry of NiO electrode on sensing performance are studied. Results show that a fast gas transport is much beneficial to improved sensitivity. NiO of porous structure is much more sensitive to CO than that of dense structure. But t_{90} (time to achieve 90% final signal magnitude) of the former is much longer due to slow gas diffusion inside the pores. It's worth noting that NiO sensor exhibits a positive relationship with CO content, opposite to other reported results of mixed potential sensors to CO. We find that it might be due to the electrochemical reduction, instead of oxidation of CO during the interaction with NiO at 1000 °C. Selectivity tests on how CO_2, CH_4 and steam affect CO sensing are also demonstrated. NiO is insensitive to even 10% CO_2. CH_4 does not shift the average value of CO sensing response. However, it makes the sensing signal fluctuate more intensively. 2% steam exerts a great influence on NiO's sensitivity to CO: it magnifies the sensitivity of porous NiO electrode to low CO range of 0-100 ppm, but inhibits that of 100 ppm to 1000 ppm. Finally, the 11-day stability test demonstrates the promising stability property of the proposed NiO-based YSZ sensor.

Introduction

With the global demand of energy expected to grow due to the population growth and progressive industrialization, the amount of renewable energy would not be adequate to meet the demand.[1] Fossil fuel (coal, oil and natural gas) would continue to play an important role in the global energy landscape for the foreseeable future.[2, 3] Thus, with the fast-growing environmental and economic pressures as the world is shifting towards a low-carbon energy transition,[4] fossil fuel-based combustion processes, especially the electricity/heat generation that accounts for a large portion of total CO_2 emission,[5] should perform with higher efficiency and minimum emission.

Upgrading combustion control system is an effective method to improve the combustion efficiency because it can monitor and adjust the firing process in real-time to minimize the heat loss.[6] It was reported that at Calaveras Power, JK Spruce Station, the heat rate and boiler efficiency was improved by 1.08% and 0.93%, respectively, after using a smart optimization technology.[7] However, the current combustion control is relatively far from satisfactory, especially for that in large-scale boilers in industry, such as boilers in coal-fired power plants. It is because in addition to depending on data analytics and process control algorithm, advanced combustion control system heavily relies on the quality of the actuator and sensor network. Unfortunately, there is still a lack of well-functioning in-situ sensors for working conditions that are extremely aggressive.[8] An ideal scenario for in-situ sensors is that they can work in the temperature range of 1000-1500°C and they are deployed across the whole boiler, since the combustion process is not uniform among local areas. If the local variations of combustion can be monitored in real time, the specific burners can be adjusted to respond to local deficient combustions. At the meantime, good sensitivity, durability and fast response time are expected, in spite of the presence of poisoning ashes, dusts and gases. Cost-effectiveness is also a consideration if successful, numerous sensors would be used for the power plant fleet all over the world.

Currently, continuous emissions monitoring systems (CEMS) using pollutant analyzer, algebra conversion equations or computer program to evaluate the gas or particulate specifics offers strong benefits to the power plant operation.[9] But they are expensive and require 1) the extraction of flue gas from the boiler, 2) the use of gas filters or traps, and 3) trained personnel to correctly handle the monitoring, which add a delay between the measurement and the real-time dynamic combustion.[10] Calorimetric analyzers using resistivity temperature detectors to detect the heat of oxidation from a catalyst layer have only been demonstrated as an extractive approach, which is not especially suitable for real-time boiler control.[8] Optical sensing approaches, e.g. tunable diode or quantum

[a] Mechanical & Aerospace Engineering Department, Benjamin M. Statler College of Engineering & Mineral Resources, West Virginia University, Morgantown, WV 26506, USA. E-mail: Xingbo.liu@mail.wvu.edu
School of Materials Science and Engineering, Hebei University of Engineering, Handan 056038, China
‡These authors contributed equally to this work.
Electronic Supplementary Information (ESI) available: [details of any supplementary information available should be included here]. See DOI: 10.1039/x0xx00000x

cascade laser spectroscopies are still not reliable enough given that a large amount of substances impede light transmission and the measured value is not local but an average one among the light path.[11]

Chemical resistive sensors based on carbon materials and semiconducting polymer and oxides are used widely for gas sensing at relatively lower temperature(<500 ^{o}C).[12-16] They have many advantages, such as cost effectiveness, high sensitivity and capability of miniaturization.[17] However, the lack of selectivity to some combustible gases and insufficient long-term stability at extremely high temperature may be the problem. Fossil fuel sources are amenable to the use of high-temperature, oxygen ion-conducting solid electrolytes such as yttrium-stabilized or calcium-stabilized zirconium oxide (YSZ or CSZ) mixed potential sensors to enable closed-loop combustion control. However, many YSZ-based mixed potential-type sensors reported are not suitable for the in-situ sensing in utility boilers because they consist of metallic sensing electrodes.[18] At high temperatures, very similar catalytic kinetics on different metallic electrodes makes it difficult to establish an obvious mixed potential response.[19] There barely are reported literatures on the development of mixed potential-type YSZ-based sensor at temperatures higher than 900^{o}C to monitor combustion process.

At present, the combustion process monitoring is mostly accomplished by monitoring oxygen alone. However, a more accurate approach would be the concurrent measurement of the CO and oxygen concentration. The optimum condition for boilers in a coal-fired power plant is to operate in around 1-2% O_2 and 100-200 ppm CO depending on fuel type, which is near the stoichiometric point with the highest efficiency in safe operation.[8] In this work, we investigated NiO as the sensing material toward hundreds of ppm CO under the conditions of 0.5%-3% O_2 at 1000 ^{o}C. The effects of flowrate of sample gas, geometry and structure of NiO electrode on the response magnitude and time were systematically studied. A one-of-a-kind YSZ-based mixed potential sensor with NiO sensing electrode was achieved, showing a response as high as 36 mV to 1000 ppm CO at 1000^{o}C. The sensing stability was also demonstrated via a 11-day continuous testing.

Experimental Section

Sensor fabrication

The mixed potential-type sensor structure is shown in Fig. 1(a), which consists of an 8YSZ electrolyte, a NiO and a porous Pt electrode in the sensing side, and another Pt electrode at the reference side. A dense circle YSZ pellet with a diameter of 2.5 cm and thickness of 0.2 cm was fabricated at first by mechanical pressing of YSZ powder (Tosoh-zirconia TZ-8YSB) followed by 1400^{o}C sintering at air for 4 h. Then each circular electrode was made one by one by screen-printing the electrode material slurries onto the electrolyte followed by 1400 ^{o}C annealing in air for 4 h. NiO slurry was made by mixing the commercial NiO powders (Fuelcellmaterials NiO-F) and an organic vehicle. Pt slurry was supplied by ESL ElectroScience Inc. The RefPt (Pt electrode in the refereynce side) electrode was 1.5 cm in diameter, while two sensing electrodes, NiO and SenPt (Pt electrode in the sensing side), were 0.5 cm in diameter. Two different morphologies of NiO electrode, dense and porous, were prepared. X-ray diffraction (XRD, PANALYTICAL X'Pert Pro) with the 0.02^{o} step size was used to characterize the as-prepared NiO electrode, confirming the crystalline structures of NiO and YSZ that show no reactivity between them. Scanning electron microscope (SEM Hitach S-4700) was used to characterize their micro-morphologies of each electrode. Brunauer, Emmett and Teller (BET) surface area analysis (Micromeritics, RSAP 2020 Plus) was conducted to determine the electrode surface area and porosity.

Sensor packaging and lab-test station

Two-compartment configuration for lab-test, as shown in Fig. 1(c), was made via using two identical silica tubes (Advalue Technology LLC) pressing against the sensor pellet. Mica O-rings were positioned between SiO_2 tubes and the sensor pellet to obtain a good sealing. The outside diameter of the silica tubes matched the diameter of the sensor pallet. In the sensing side, an Al_2O_3 tube was flowing the mixed gases that consist of 2000 ppm CO gas, N_2 and air, in which the gas components were controlled by adjusting its mass flow rate by digital mass controllers (Alicat). For example, 0 ppm CO and 2%O_2 sample gas (200 sccm total flowrate) is from 20 sccm air + 0 sccm 2000 ppm CO bal. N_2 + 180 sccm N_2. 1000 ppm CO and 3%O_2 sample gas ((200 sccm total flowrate)) is from 30 sccm air + 100 sccm 2000 ppm CO bal. N_2 + 70 sccm N_2.On the reference side, an Al_2O_3 tube was used to feed air.

All gases were supplied and graded as ultra high purity by Matheson Gas Inc; the detailed compositions of gases are shown in Table 1 in **SI**. A multi-channel Gamry electrochemical workstation was applied to simultaneously record the voltage signals, with the working electrodes connected to NiO electrode and Pt electrode on the sensing side, and reference electrode connected to Pt electrode on the reference/air side.

Gas-sensing properties measurements

The response of the sensor was measured in the atmosphere of 0-1000 ppm CO and 0.5%-3% O_2 balanced by N_2 with a total 200 sccm (standard cm^3/min) flowrate at temperature of 1000^{o}C. NiO and Pt at sensing side (SenPt) were exposed to the sample gas while Pt electrode at reference side (RefPt) was always exposed to air. Two potentials were recorded: NiO vs. RefPt (V_{NiO}) and SenPt vs. RefPt (V_{SenPt}). The magnitude of response (ΔV) was defined as the potential differences between sample gases and the base gas. For example, the response of NiO to 100 ppm CO is ΔV_{NiO}(100 ppm) = V_{NiO}(100 ppm)-V_{NiO}(0 ppm). t_{90}, 90% response time, was defined at the duration to reach 90% value of ΔV in gas composition shift. Selectivity tests were also conducted for CO_2, steam and CH_4.

Results and discussion

Morphologies of sensor electrodes

Fig.2 shows SEM photographs of the cross-sections of as-prepared dense NiO electrode/YSZ interface, porous NiO/YSZ interface and SenPt/YSZ interface, with the thickness of each electrode shown. It is seen from Fig. 2(a) that although some defects exist over the surface, the NiO film is quite dense. Therefore, we assume that most sensing signal of the dense NiO electrode comes from the TPB (three-phase boundary), which is the outer circle of the contact of dense NiO electrode, YSZ and sample gas. Fig. 2(c) is the morphology of a porous

Pt electrode, representative of both SenPt and RefPt for they were made through the same process. The surface area and porosity of the porous and dense NiO was further measured via BET analysis. The detailed BET sample preparation procedure and the results are shown in Fig. S1 and Fig. S2. Fig. S2(a), (b) and (d) show that the surface area and pore size of porous NiO is 1.33 m^2/g and 65 nm, respectively. In contrast, as shown in Fig. S2(c), the quantities of adsorbed nitrogen for the dense NiO are negative numbers, which is not valid data. This is because the surface area is too small and lower than the detection of limit of the BET instrument .

CO sensing behavior of NiO electrodes

Mixed potential on an electrode is established via at least two competing redox reactions occurring on the electrode, where due to zero net current and charge conservation, an electrochemically steady-state condition is achieved leading to a measurable mixed potential.[20, 21] Fig. 3 (a)-(c) show the typical sensing behaviors to CO for dense and porous NiO electrodes and SenPt electrode, in atmospheres varying between 0-1000 ppm CO and 0.5%-3% O_2 at 1000°C with the total sample gas flowrate of 200 sccm. SenPt does not show obvious sensitivity to CO and potentials are very close to the theoretical Nernst potential (Nernst: -53mV for 3% O_2 at 1000°C). It is primarily due to the fact that at temperature as high as 1000°C, the heterogeneous catalytic CO-O_2 reaction over metallic electrode surfaces is very fast, and very few CO reaches the TPB area. If some CO reaches TPB, the electrochemical activity of metallic electrode towards oxygen reduction reaction is so high that the mixed potential would not deviate much from its equilibrium oxygen potential. Both factors contribute to the low sensitivity to CO for the SenPt electrode at 1000 °C.

In contrast, both dense NiO and porous NiO electrode exhibit obvious sensing ability to CO at 1000°C and 0.5%-3% O_2, as seen in Fig. 3(a), (b), (d) and (e). Although the porous NiO demonstrates superior sensitivity to CO as shown in Fig. 3(b), its response time (t_{90}=254s) is not so good as that of the dense NiO (t_{90}=14s). This is likely because the porous structure experienced a slow gas transport process, prolonging the transition time to the stable state. Fig. 3(f) summerizes the relationship of t_{90} with oxygen concentration for dense and porous NiO electrode. T_{90} for porous NiO tends to increase with the increased oxygen content, while t_{90} for dense NiO does not have a definite dependence on oxygen. For dense NiO, gas transport is not a limiting step given the 200 sccm flowrate, therefore t_{90} reflects the electrochemical reaction kinetics. Since CO is at ppm level, the limiting step for electrochemical reactions should be related to CO rather than oxygen concentration, leading to the T_{90} of dense NiO insensitive to oxygen concentration change. In contrast, for porous NiO electrode, higher oxygen concentration results in less CO reaching the sensing-active sites because the longer residence time leads to more thorough heterogeneous reaction between CO and O_2. This further slows the diffusion of CO due to the decreased CO concentration gradient. Fig. 3(d) and (e) exhibit the relationship between sensing response (ΔV) and CO concentration. For dense NiO, it basically shows the linear relationship of ΔVs with the logarithm of CO, although in the case of 2% O_2, a good linearity is only seen for CO content ranging from 200 ppm to 1000 ppm. This supports the hypothesis that electrochemical reaction, instead of gas diffusion, is the rate-limiting step for the dense NiO electrode. In contrast, the non-linearity is relatively more dominant for the porous NiO electrode, which reveals that the gas diffusion plays a role in the sensing kinetics.

It is noteworthy that there is a positive relationship between the sensing response and CO concentration for NiO electrode as seen in Fig. 3(d) and (e). This phenomenon is opposite to other published results in works of mixed potential-type CO sensor.[22-25] Mixed potential of an electrode is known to be established via electrochemical redox reactions occurring over the electrode. For scenarios that are commonly seen in literature, the mixed potential is formed due to CO oxidation and oxygen reduction, as illustrated by the black lines in Fig. 4(a). In this case, the mixed potential will go negatively with the increasing CO content. However, in this present work, we find that the measured mixed potential is increasing when the CO concentration goes up. Therefore, as shown by the red lines in Fig. 4(a), there should be a CO-involved reduction reaction occurred over the NiO surface, because only cathodic reactions can cause the mixed potential to increase. We think that the reduction of CO to carbon and oxygen ions is one possibility. Fig. 4(b) shows that the calculated Gibbs free energies for the formation of C and CO from CO_2 in standard condition defined in NIST-JANAF table.[26, 27] The standard ΔG of CO → C+ ½ O_2 can be obtained by using the red line minus the green line. We can see that when the temperature is over 700°C, the Gibbs free energy of CO reduction to carbon and oxygen is negative, indicating that CO tends to decompose into carbon and oxygen. Of course, many factors have to be considered when we discuss thermodynamics, such as the partial pressure of each component and the involved possible reactions. To test this hypothesis of CO reduction, we measured the signal changes of the porous NiO electrode at different temperatures from 700°C to 1000°C with other conditions unchanged, as shown in Fig. 4(c)-(f). It is obvious that below 900°C, the sensing behavior shows a negative correlation of the measured signal and CO concentration. However, when the temperature rises to 900°C or higher, the opposite behavior occurs. This reversion at some extent supports our hypothesis that CO reduction may happen at higher temperatures and suggests that 900°C may be the break-in point at which CO reduction starts to occur.

To further elucidate the possible mechanism, polarizations were conducted at different CO content and 800°C and 900 °C and 2% O_2 for a porous NiO sensor sample, as shown Fig. 5(a) and (b). The OCV values under each CO content show the same trend with the results in Fig. 4 (e) and (f). For the polarization regions, a reversed response of NiO to CO can be observed by rising temperature from 800 to 900 °C. At 800 °C, the anodic current increases with the increase of CO content, while at 900 °C, the anodic current decreases with increase of CO. This is because CO at 800 °C is a combustible. Thus, a higher CO content would lead more CO to be oxidized at the same potential, resulting in higher net current. In contrast, at 900 °C, if CO is supposedly being reduced, the anodic polarization would suppress the CO reduction reaction, leading to a smaller net current. The similar idea applies for the cathodic polarization regions. At 800 °C, CO oxidation is suppressed during the cathodic polarization, while at 900 °C, CO reduction is prompted when cathodically polarized.

Fig. 5(c) and (d) presents the XRD results for as-prepared porous NiO sensor and the sensor after annealed at 1000 ppm CO + 2%O_2

bal. N_2 for 3 days. The NiO peaks and YSZ peaks are sharp for both samples, indicating that the majority of the materials remain unchanged. There is a slight down-shift for the peaks from the ppm CO treated sample. It is because that after annealed at 2% O_2, NiO lost oxygen, making the lattice structure to expand. What noteworthy is that after the annealing, there are some small new peaks, as clearly shown in Fig. 5(d), magnified figure of 5(c). There are small foreign peaks in the angle range of 20° to 28°. We cannot identify exactly what are these peaks. However, the highest one at 25.6° is close to the standard peak of (002) graphite peak of 26.2°.

To confirm the mechanism of this opposite signal, more efforts in morphology characterizations and even theoretical calculations will be put on our future work.

Fig. 6(a) and (c) demonstrate the effect of gas transport on the CO sensing behavior of porous NiO at 3% P_{O2} and 1000°C. While the sample gas composition and total flowrate were kept unchanged, the gas transport was adjusted by changing the positions of the gas tube outlet as shown in Fig. 6(a). The highest sensitivity to CO is obtained for the case that the gas tube was placed in position 1, the nearest distance to sensor surface. It's not surprising to see such an influential effect of the CO transport to the sensitivity of porous NiO given the slow gas transport inside NiO pores can be a limiting factor. The response reached as high as 36 mV for 1000 ppm CO for the case of position 1, which suggests a strong interaction between CO and NiO given at 1000°C oxygen reduction reactions are expected to be strong as well. Some performance comparison with results in literature is shown in Table 2 in **SI**. Fig. 6(b) and (d) reveal how the geometry of NiO electrode affects the sensing behavior. Large area porous NiO has better sensitivity but longer response time than the small area one. This result is understandable because more time is needed for the larger electrode to reach a stable state. However, for the relationship between electrode area and the sensitivity to CO, one shouldn't draw a conclusion of the larger the area, the higher the sensitivity, because sensitivity cannot be improved without limit just by enlarging electrode area. We believe this phenomenon has more to do with the 2D gas flow distribution relative to the electrode and the kinetics of CO reaction.

Selectivity over other possible combustion gases

Selectivity to CO over other major gas components in the utility boiler, such as CO_2, steam and hydrocarbons, is important. The effect of CO_2 on the sensing performance of CO is shown in Fig. 7(a). The red dash line indicates a change from 10% CO_2 to 0% CO_2. 10% CO_2 barely has any effect on the response, which means a very low selectivity of porous NiO electrode to CO_2. This result reveals that either the absorption of CO_2 is fairly low or CO_2 doesn't participate in the electrochemical reactions to build mixed potential, which is coincident with our speculation that CO is reduced to C and O^{2-} instead of oxidized to CO_2 on NiO. The effect of CH_4 on the sensing performance of CO is shown in Fig. 7(b). It is seen that CH_4 in the atmosphere increases the signal fluctuation. However, CH_4 doesn't change the average sensing response to CO. Furthermore, after shutting off CH_4, the fluctuation starts to fade out which means the effect of CH_4 on the CO sensing is reversible.

The effect of H_2O on the sensing performance of CO is shown in Fig. 7(c) and (d). The only difference between Fig.7(c) and (d) is the total sample gas flowrate. In Fig. 7(c), the sensitivity to CO was greatly reduced due to the existence of 2% steam. The total flowrate was increased to improve the sensitivity according to the results shown above about the beneficial effect of flowrate. It is seen in Fig. 7(d) that above 100 ppm CO, the sensitivity is relatively low. In contrast, the NiO electrode shows greatly improved sensitivity to the low CO content range (0-100 ppm) compared to atmosphere without steam in Fig. 3 (a) and (b). One possibility is that the coverage of H_2O-related absorbates is high, leading to an easily saturated CO absorption, thus making the electrode less sensitive to higher CO contents.

Sensor Stability demonstration

Fig.8(a) presents the initial sensing behaviour to CO at 2% O_2 and 1000 °C for a porous NiO sensor sample that is used to operate for a stability test as shown in Fig. 8(b). Fig. 8(b) shows the 11-day stability test for the porous NiO sensor to 200 ppm CO at 1000 °C and 2%O2. During this period of time, although a bit larger fluctuation occurred after day 5, the sensor showed overal good stability, demonstrating its good potential for a long-term run.

Conclusions

In this work, we found NiO was a promising material for in-situ high temperature CO sensing in utility boilers, such as coal-fired power plants. Its characteristics of enduring temperature as high as 1000 °C and good sensitivity, selectivity and response time to CO made it an excellent candidate for combustion monitoring sensor integrated into smart control system. Under the conditions of 0.5%-3% O_2 and 1000 °C, the fabricated YSZ-based mixed potential sensor using porous NiO showed good sensitivity to ppm-scale CO. It showed a signal as high as 36 mV to 1000 ppm CO. In addition, how the sample gas transport and NiO electrode's structure and geometry affect the sensing behavior was studied. Results showed that sensitivity could be improved by facilitating gas diffusion. Porous NiO had higher sensitivity to CO than dense NiO. But in the meantime, the porous structure resulted in much longer response time. Selectivity tests on the effects of CO_2, CH_4 and steam on CO sensing were also conducted. NiO was insensitive to even 10% CO_2. CH_4 has not shifted the average value of CO sensing response. However, it made the sensing process unstable due to the enlarged signal fluctuation. 2% Steam exerted a great influence on NiO's sensing: porous NiO electrode showed relatively small variations with the CO content changing from 100 ppm to 1000 ppm; in contrast, the sensitivity of porous NiO electrode to low CO range of 0-100 ppm was enhanced significantly. This may be due to the decreased number of available adsorption sites for CO, which is preferrably occupied by H_2O-related species, making the CO-related absorbates easily saturated when CO content is higher than 100 ppm. It's worth noting that the potential of NiO exhibited a positive relationship with CO content. This is opposite to nearly all reported results in the works of mixed potential sensors to CO. We found it might be due to the electrochemical reduction of CO during the interaction with NiO at 1000 °C rather than being oxidized. Finally, the 11-day stability test to 200 ppm CO at

2%O_2 and 1000 °C demonstrates its promising potential of stable performing.

Conflicts of interest

There are no conflicts to declare

Acknowledgements

This investigation is funded by U.S. Department of Energy, National Energy Technology Laboratory (NETL) under the contract number DE-FE31564. We would like to thank the program managers Drs. John Rockey, Sydni Credle, Barbara Carney for the technical guidance and financial support. We also acknowledge the use of the WVU Shared Research Facilities and managers Drs. Qiang Wang and Marcela Redigolo. We also acknowledge the use of BET instrument and managers Dr. Kostas Sierros, Dr. John Hu, Mr. Domenic Cipollone and Ms. I-wen Wang.

References

1. Z. R. Chong, S. H. B. Yang, P. Babu, P. Linga and X.-S. Li, *Applied Energy*, 2016, **162**, 1633-1652.
2. M. Ball and M. Wietschel, *International Journal of Hydrogen Energy*, 2009, **34**, 615-627.
3. R. F. Aguilera and R. Aguilera, *Mineral Economics*, 2019, DOI: 10.1007/s13563-019-00192-5.
4. G. Wood, in *The Palgrave Handbook of Managing Fossil Fuels and Energy Transitions*, Springer, 2020, pp. 3-23.
5. IEA, *CO2 Emissions from Fuel Combustion 2019*, IEA, Paris, 2009.
6. N. Docquier and S. Candel, *Progress in Energy and Combustion Science*, 2002, **28**, 107-150.
7. J. Sutton and P. Spinney, 2016.
8. P. Shuk and C. McGuire, *Sensors & Transducers*, 2017, **217**, 1-13.
9. F. Liu, B. N. Duncan, N. A. Krotkov, L. N. Lamsal, S. Beirle, C. A. McLinden, D. Griffin, D. L. Goldberg and Z. Lu, *AGUFM*, 2019, **2019**, A44E-07.
10. J. Kamas and J. Keeler, 1995.
11. P. Shuk, C. McGuire and E. Brosha, *Sensors & Transducers*, 2019, **229**.
12. L.-S. Zhang, L.-Y. Jiang, C.-Q. Chen, W. Li, W.-G. Song and Y.-G. Guo, *Chemistry of Materials*, 2010, **22**, 414-419.
13. W. Li, L.-S. Zhang, Q. Wang, Y. Yu, Z. Chen, C.-Y. Cao and W.-G. Song, *Journal of Materials Chemistry*, 2012, **22**, 15342-15347.
14. Y. Lu, W. Li, J. Zhang, Y. Liu, P. Casey, S. Bateman, S. Z. Shen, J. Zhou, G. S. Zakharova and W. Chen, *Ferroelectrics*, 2015, **477**, 93-102.
15. R. Purbia, Y. M. Kwon, H.-D. Kim, Y. S. Lee, H. Shin and J. M. Baik, *Journal of Materials Chemistry A*, 2020, **8**, 11734-11742.
16. D. Wang, Y. Yin, P. Xu, F. Wang, P. Wang, J. Xu, X. Wang and X. Li, *Journal of Materials Chemistry A*, 2020, **8**, 11188-11194.
17. Y. Liu, J. Parisi, X. Sun and Y. Lei, *Journal of Materials Chemistry A*, 2014, **2**, 9919-9943.
18. X. Zhang, H. Kohler, M. Schwotzer, Y. Wu and U. Guth, *Sensors and Actuators B: Chemical*, 2019, **278**, 117-125.
19. H. Okamoto, H. Obayashi and T. Kudo, *Solid State Ionics*, 1980, **1**, 319-326.
20. T. Ritter, J. Lattus, G. Hagen and R. Moos, *Sensors and Actuators B: Chemical*, 2019, **287**, 476-485.
21. N. Miura, T. Sato, S. A. Anggraini, H. Ikeda and S. Zhuiykov, *Ionics*, 2014, **20**, 901-925.
22. S. A. Anggraini, Y. Fujio, H. Ikeda and N. Miura, *Analytica Chimica Acta*, 2017, **982**, 176-184.
23. K. Mahendraprabhu, A. Selva Sharma and P. Elumalai, *Sensors and Actuators B: Chemical*, 2019, **283**, 842-847.
24. N. D. Tho, D. V. Huong, H. T. Giang, P. Q. Ngan, G. H. Thai, D. T. A. Thu, D. T. Thu, N. T. M. Tuoi, N. N. Toan, P. D. Thang and H. N. Nhat, *Electrochimica Acta*, 2016, **190**, 215-220.
25. M. Yamaguchi, S. A. Anggraini, Y. Fujio, M. Breedon, V. V. Plashnitsa and N. Miura, *Electrochimica Acta*, 2012, **76**, 152-158.
26. J. Lau, G. Dey and S. Licht, *Energy Conversion and Management*, 2016, **122**, 400-410.
27. M. W. Chase Jr, *J. Phys. Chem. Ref. Data, Monograph*, 1998, **9**.

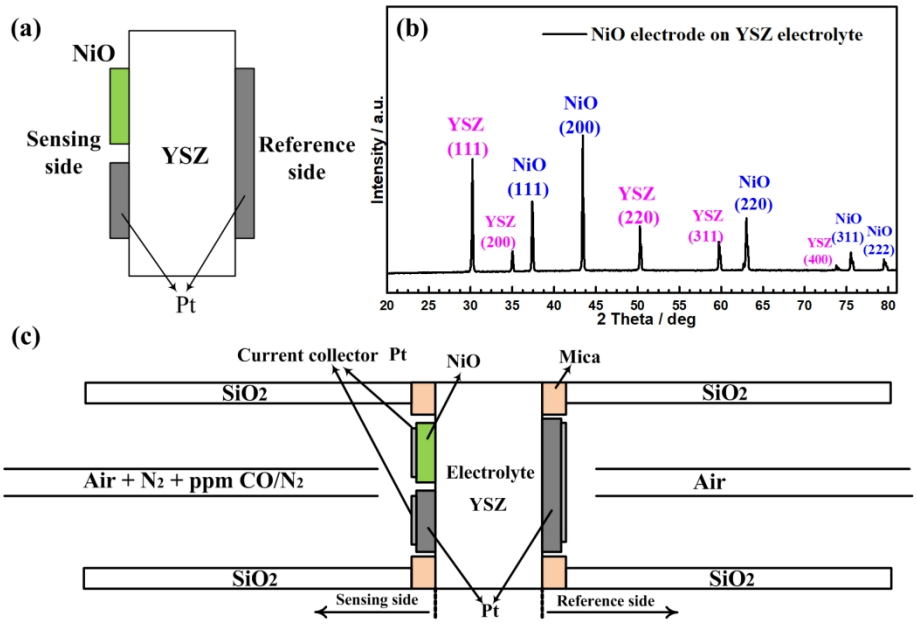

Fig. 1 (a) structure of the YSZ-based mixed potential sensor consisting of YSZ electrolyte, NiO sensing electrode, Pt sensing electrode and reference electrode. (b)XRD of the porous NiO electrode for the as-prepared sensor sample (c) lab test configuration for the CO testing for all lab-test results presented in this work.

184x122mm (256 x 256 DPI)

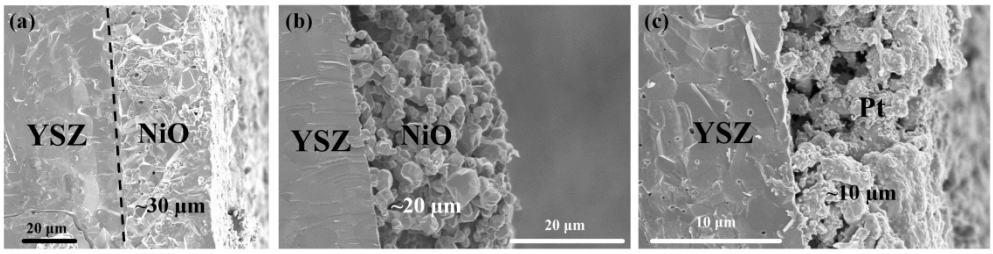

Fig. 2 SEM images of cross-sections of YSZ electrolyte and (a) dense NiO electrode, (b) porous NiO electrode and (c) porous Pt electrode

320x87mm (222 x 222 DPI)

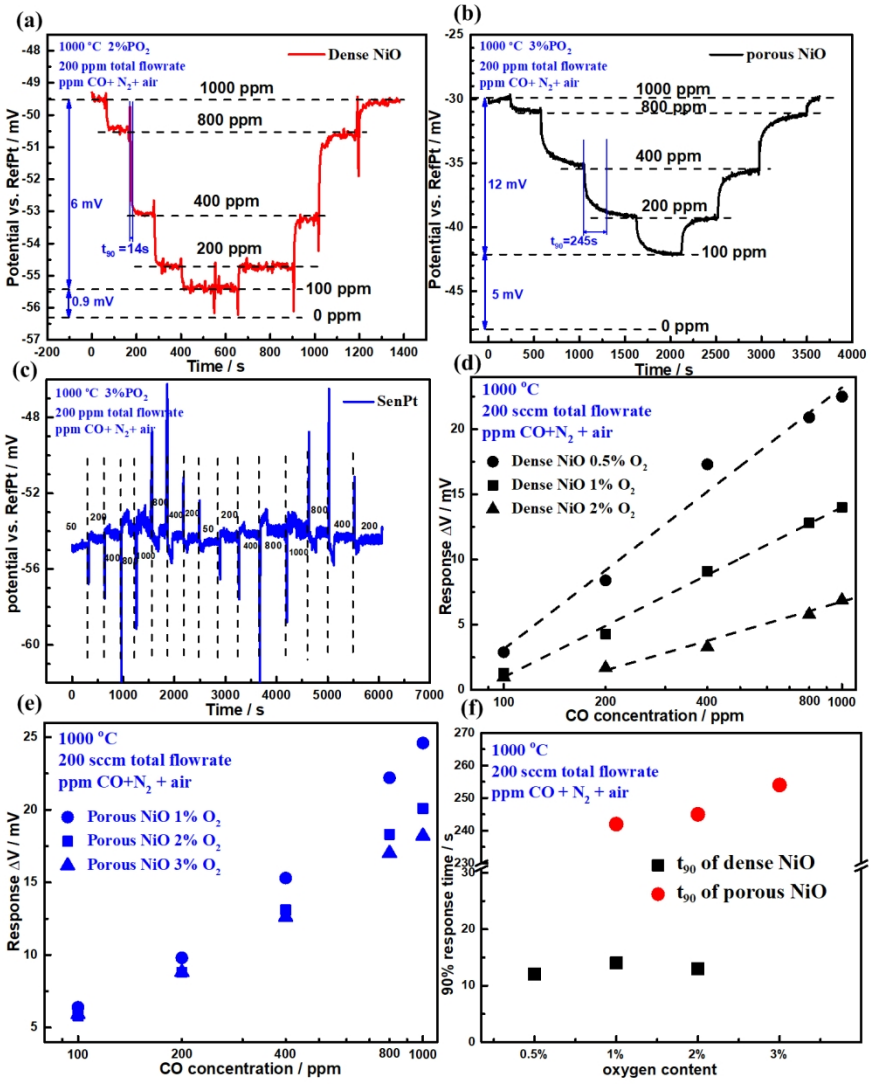

Fig. 3 Sensing behavior to CO of, (a) dense NiO, (c) porous NiO, (c) SenPt, at atmospheres varying between 0-1000 ppm CO and 2%-3% O_2 at 900°C and 1000°C with the total flowrate of 200 sccm. The sensing response (ΔV) to CO concentration for (d) dense NiO and (e) porous NiO. (f) The relationship of 90% response time t_{90} with oxygen content for both dense and porous NiO.

214x242mm (200 x 200 DPI)

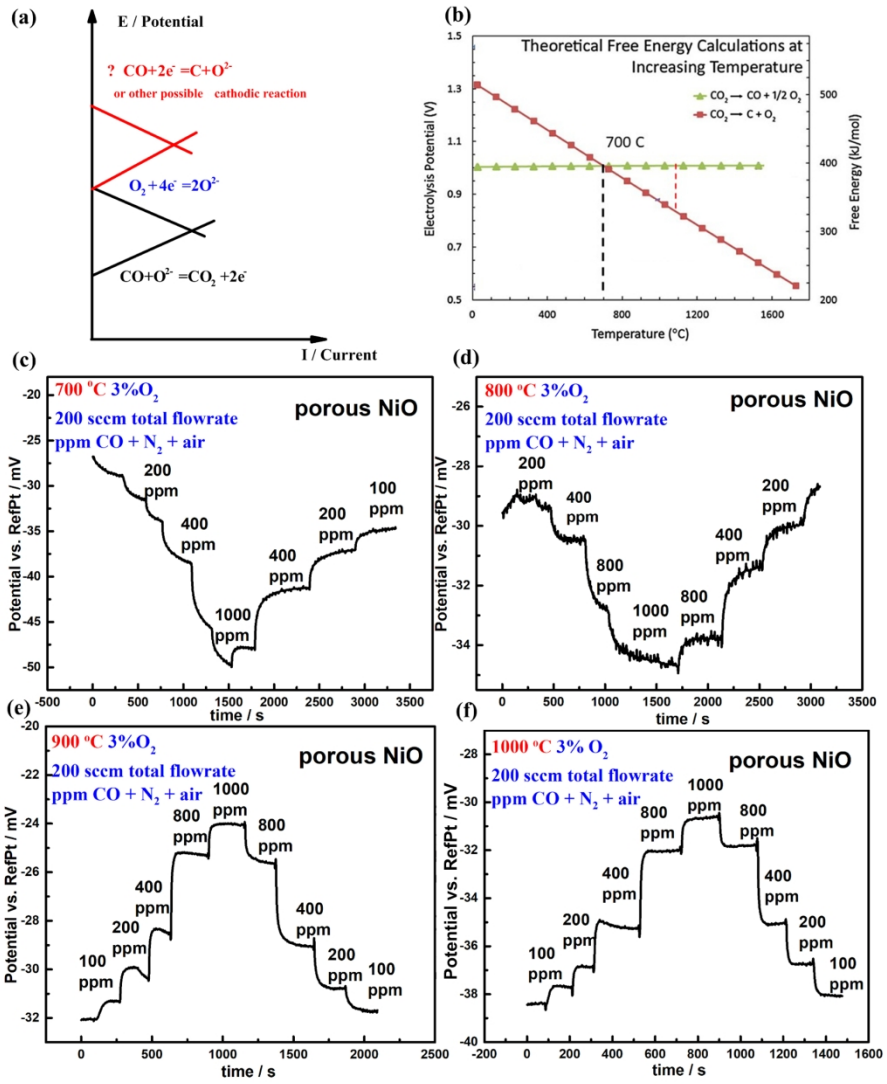

Fig. 4 (a) the schematics of the establishment of mixed potential of an electrode. (b) theoretical calculation of free energy for CO_2 reduction to carbon and carbon monoxide[26,27] (c)-(f) CO sensing testing for porous NiO in different temperature from 700 ^{o}C to 1000 ^{o}C

558x626mm (96 x 96 DPI)

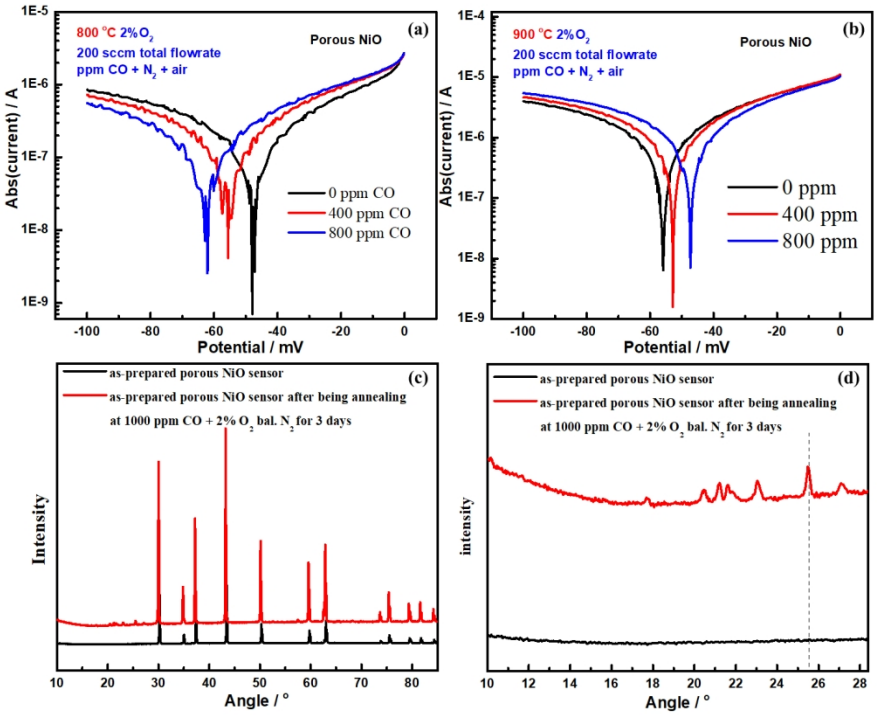

Fig. 5 The polarization curve at different CO content and 2% O_2 for one porous NiO sensor sample at (a) 800 ^{o}C and (b) 900 ^{o}C. (c) Full spectrum of XRD of the as-prepared porous NiO and the same sensor after annealing at 1000 ppm CO + 2%O_2 bal. N_2 for 3 days (d) Magnified region for the range of 10^{o} to 28^{o}

192x150mm (222 x 222 DPI)

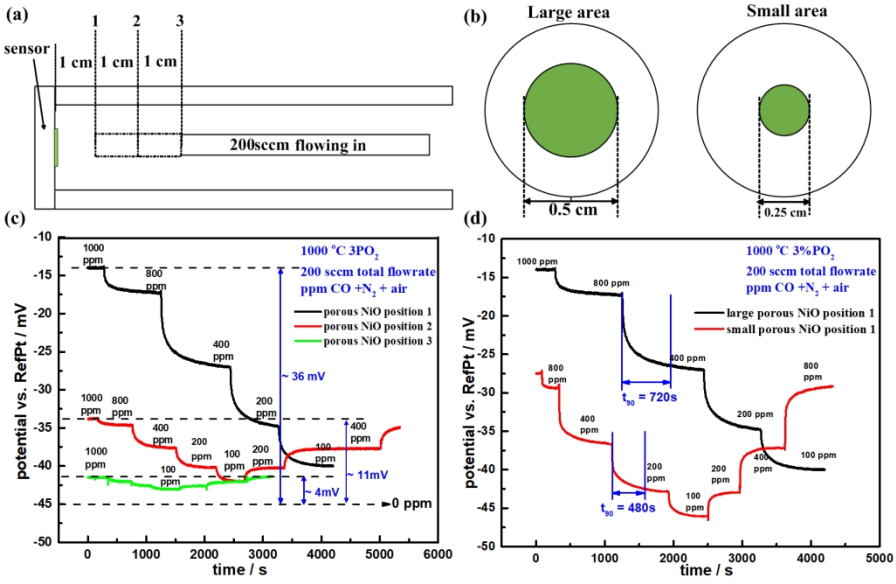

Fig. 6 (a) and (c) the effect of gas transport on the CO sensing behavior of porous NiO at 3% PO_2 and 1000 ^oC. (b) and (d) the effect of electrode geometry on the sensing behavior

218x135mm (222 x 222 DPI)

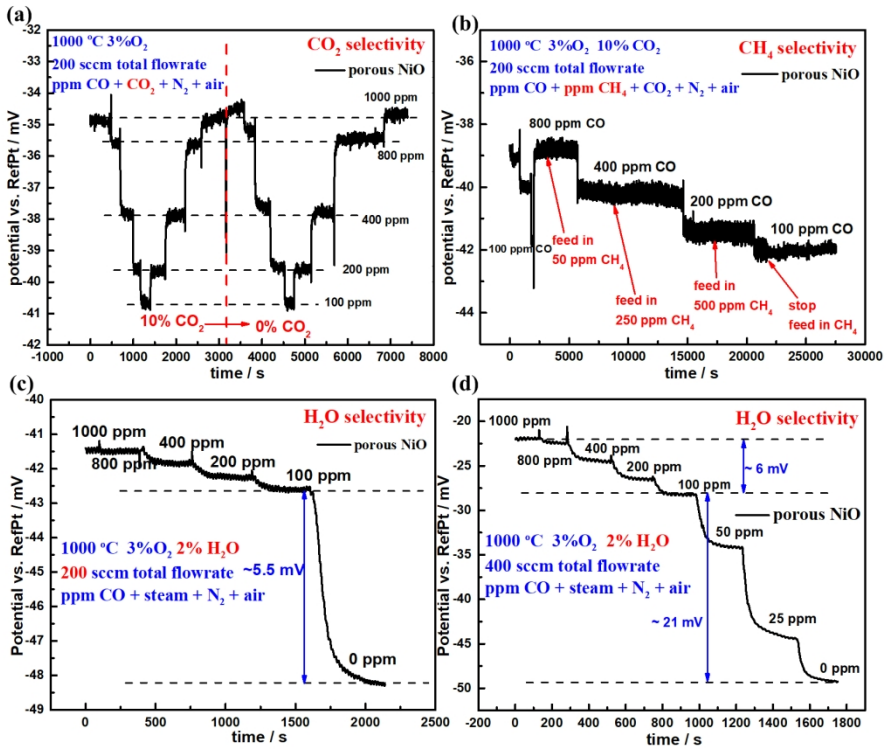

Fig. 7 CO sensing tests of porous NiO electrode at 1000 ^{o}C and 3% O_2 when including the effect of other gases (a) 10% CO_2 (b) ppm-scale CH_4 (c) 2% H_2O with 200 sccm total flowrate and (d) 2% H_2O with 400 sccm total flowrate

219x176mm (222 x 222 DPI)

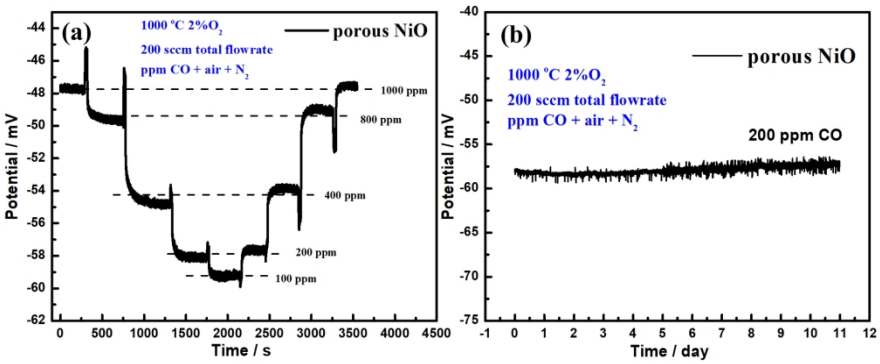

Fig. 8 (a) The initial sensing behavior to CO at 2% O_2 and 1000 ^{o}C before a stability test. (b) the 11-day stability test for the porous NiO sensor to 200 ppm CO at 1000 ^{o}C and 2%O_2

190x82mm (300 x 300 DPI)

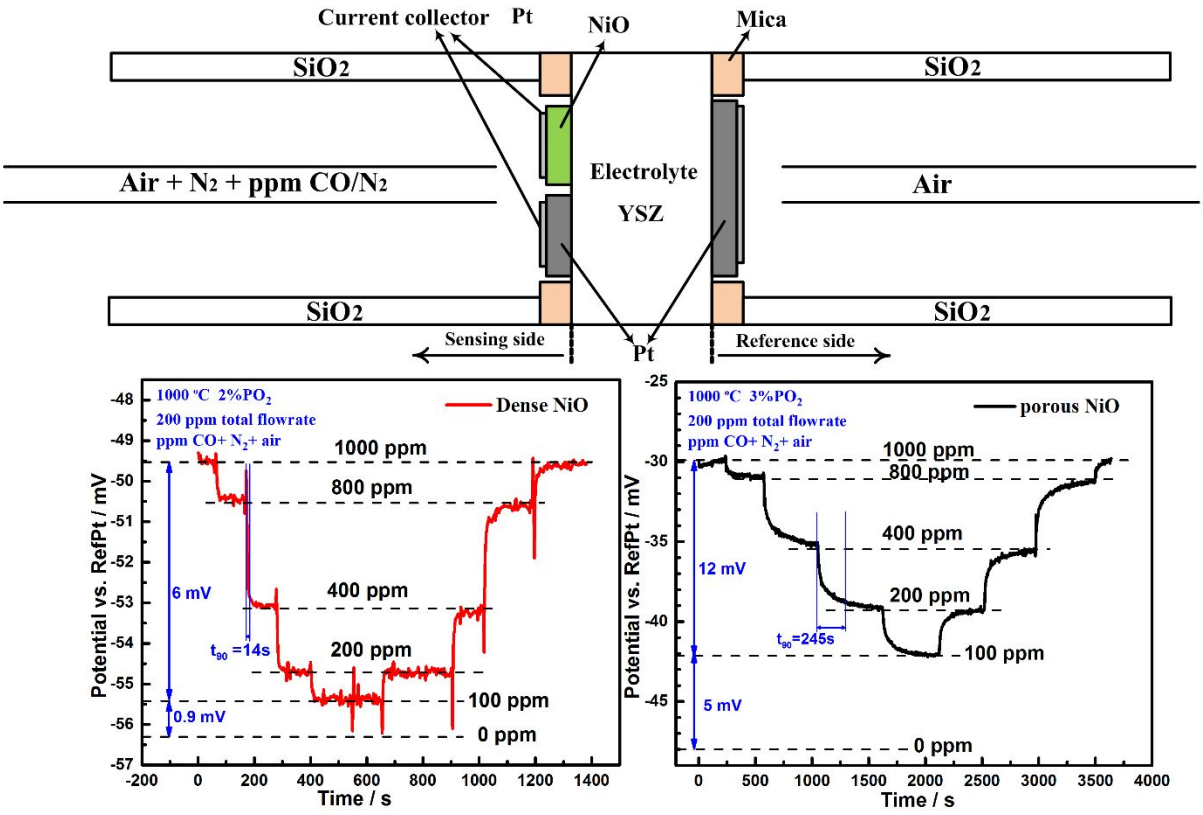

NiO electrodes of mixed potential YSZ sensors show a positive potential feedback to CO with high sensitivity at 1000 °C